# Optical transmission spectrum of incommensurate crystals: Application to $Rb_2ZnBr_4$

G. Wahlström and K. A. Chao
*Department of Physics and Measurement Technology, University of Linköping, S-58183 Linköping, Sweden*
(Received 20 April 1987; revised manuscript received 29 June 1987)

We have analyzed the optical transmission spectrum of an incommensurate crystal using a three-dimensional tight-binding model with modulation along one direction. When the theory is applied to $Br_2ZnBr_4$, the calculation reproduces the main features of observed change of spectrum across the normal-to-incommensurate transition at 355 K.

## I. INTRODUCTION

Among the materials which exhibit incommensurate periodic properties, $Rb_2ZnBr_4$ has remarkable temperature-dependent structure phase transitions.[1,2] At a high temperature $T>355$ K, $Rb_2ZnBr_4$ has well-defined translational symmetry and is in the so-called normal phase.

When the temperature is lowered towards 355 K, a phonon mode with wave vector $\mathbf{q}$ gets soft.[3] At $T=T_I\approx 355$ K a structure phase transition occurs, driven by the $\mathbf{q}$ soft-phonon mode. Since $\mathbf{q}$ is incommensurate to the parallel reciprocal-lattice vector $\mathbf{c}^*$, the new phase is called the incommensurate phase. If $T$ is not much lower than $T_I$, the incommensurate phase is characterized by a cosine modulation of the atomic positions with temperature-dependent amplitude. However, deep in the incommensurate phase ($T$ much less than $T_I$) the modulation of the atomic position becomes very complicated and solitons appear.[1]

With further decrease of temperature, the density of solitons drops and a second structure phase transition occurs at $T=T_c$. Below $T_c$ the material regains its translational symmetry in the form of a superstructure with one of the periodicities enlarged by a factor of 3.

Although the crystal structure of the incommensurate phase has been investigated earlier by several low-energy scattering experiments,[1,4,5] the light scattering experiment with high-energy photons was performed much later in 1984.[6] The latter explores the interband optical absorption and therefore gives valuable information concerning the electronic properties of the incommensurate phase. On the other hand, there exists a large number of theoretical studies on the electronic and transport properties of the incommensurate phase, mainly in terms of the simple one-dimensional Aubry model.[7,8-14] Because of the lack of experimental data, almost all theoretical predictions cannot be checked with experiments. Perhaps the only exception is the theoretical analysis of Rasing,[6] who has used a one-dimensional incommensurate model Hamiltonian to interpretate qualitatively the measured temperature dependence of optical absorption in $Rb_2ZnBr_4$.

In this paper we will perform a quantitative study to show that a one-dimensional incommensurate model is inadequate to explain the experimental data. Instead, a three-dimensional model with a uniaxial incommensurate modulation yields the correct optical transmission spectra when comparing with experiments.

## II. THE MODEL

When the temperature is lowered toward $T_I$, the soft-phonon mode with wave vector $\mathbf{q}$ drives the normal-to-incommensurate transition, where $\mathbf{q}$ is incommensurate to the parallel reciprocal lattice vector $\mathbf{c}^*$. In other words, $q/c^*$ must be an irrational number which cannot be measured experimentally. Actually, within the experimental accuracy the measured $q/c^*$ is a rational number $\nu/N$. For example, in the temperature range $210<T<355$ K the incommensurate phase of $Rb_2ZnBr_4$ has the measured value $\mathbf{q}=0.292\mathbf{c}^*\approx(\frac{5}{17})\mathbf{c}^*$.[15,4] That is, the crystal structure of this incommensurate phase can be well approximated by a superlattice with one of its periodicities enlarged by $N$ times. This approximation is called the rational approximation, and will be adopted in the present paper.

Let $\mathbf{a}$, $\mathbf{b}$, and $\mathbf{c}$ be the primitive vectors of the normal phase. In the normal phase the single-particle Hamiltonian

$$H=p^2/2m+V(\mathbf{r}) \tag{1}$$

has the translational symmetry $V(\mathbf{r}+\mathbf{a})=V(\mathbf{r}+\mathbf{b})=V(\mathbf{r}+\mathbf{c})=V(\mathbf{r})$. Therefore, the Bloch states $\Psi_{\mu\mathbf{k}}(\mathbf{r})$ of the $\mu$th energy band can be constructed from a set of Wannier functions $\{\Phi_\mu(\mathbf{r}-\mathbf{R});\mathbf{R}=l\mathbf{a}+m\mathbf{b}+n\mathbf{c}\}$ as

$$\Psi_{\mu\mathbf{k}}(\mathbf{r})=\sum_{l,m,n} e^{i\mathbf{k}\cdot(l\mathbf{a}+m\mathbf{b}+n\mathbf{c})}\Phi(\mathbf{r}-l\mathbf{a}-m\mathbf{b}-n\mathbf{c})\ . \tag{2}$$

In the temperature region where the incommensurate phase can be treated with the rational approximation the position of the $n$th atom along the $\mathbf{c}$ axis is modulated by a cosine function $A\cos(Qn+\phi)$, where $Q=2\pi(\nu/N)$ and $\phi$ is a constant phase factor. In this case the single-particle potential $V(\mathbf{r})$ has different periodicities $V(\mathbf{r}+\mathbf{a})=V(\mathbf{r}+\mathbf{b})=V(\mathbf{r}+N\mathbf{c})=V(\mathbf{r})$. Equation (2) is then modified as

$$\Psi_{\mu\mathbf{k}}(\mathbf{r})=\sum_n e^{i\mathbf{k}\cdot n\mathbf{c}}F_{\mu\mathbf{k}}(n)\sum_{l,m} e^{i\mathbf{k}\cdot(l\mathbf{a}+m\mathbf{b})} \times\Phi_\mu(\mathbf{r}-l\mathbf{a}-m\mathbf{b}-\zeta_n\mathbf{c})\ , \tag{3}$$

 

where

$$\zeta_n = n + A\cos(Qn+\phi)\ , \tag{4}$$

and the coefficient $F_{\mu\mathbf{k}}(n)$ has the same translational symmetry $F_{\mu\mathbf{k}}(n+N)=F_{\mu\mathbf{k}}(n)$.

The Schrödinger equation

$$H\Psi_{\mu\mathbf{k}}(\mathbf{r})=E_\mu(\mathbf{k})\Psi_{\mu\mathbf{k}}(\mathbf{r}) \tag{5}$$

will be solved with the nearest-neighbor tight-binding approximation. Since the atomic positions are modulated along the c axis, the potential $V(\mathbf{r})$ is also modulated. Therefore, the matrix elements

$$\alpha_\mu(n)=\langle\Phi_\mu(\mathbf{r}-l\mathbf{a}-m\mathbf{b}-\zeta_n\mathbf{c})\,|\,H\,|\,\Phi_\mu(\mathbf{r}-l\mathbf{a}-m\mathbf{b}-\zeta_n\mathbf{c})\rangle \tag{6}$$

and

$$\gamma_{\mu\mathbf{c}}(n+1,n)=\langle\Phi_\mu(\mathbf{r}-l\mathbf{a}-m\mathbf{b}-\zeta_n\mathbf{c})\,|\,H\,|\,\Phi_\mu(\mathbf{r}-l\mathbf{a}-m\mathbf{b}-\zeta_{n+1}\mathbf{c})\rangle \tag{7}$$

depend on the value of $n$ explicitly. However, the effect of modulation on the transverse hopping matrix elements

$$\gamma_{\mu\mathbf{a}}=\langle\Phi_\mu(\mathbf{r}-(l+1)\mathbf{a}-m\mathbf{b}-\zeta_n\mathbf{c})\,|\,H\,|\,\Phi_\mu(\mathbf{r}-l\mathbf{a}-m\mathbf{b}-\zeta_n\mathbf{c})\rangle \tag{8}$$

and

$$\gamma_{\mu\mathbf{b}}=\langle\Phi_\mu(\mathbf{r}-l\mathbf{a}-(m+1)\mathbf{b}-\zeta_n\mathbf{c})\,|\,H\,|\,\Phi_\mu(\mathbf{r}-l\mathbf{a}-m\mathbf{b}-\zeta_n\mathbf{c})\rangle \tag{9}$$

are of the second order and will be ignored. In the temperature region where the modulation is given by Eq. (4), the value of $A$ is much less than one. Hence, if we make a series expansion of the matrix elements with respect to $A$ and keep only the linear term, $\alpha_\mu(n)$ and $\gamma_{\mu\mathbf{c}}(n+1,n)$ can be written in the general form

$$\alpha_\mu(n)=\alpha_{\mu0}+\alpha_{\mu1}\cos(Qn+\phi) \tag{10}$$

and

$$\gamma_{\mu\mathbf{c}}(n,n-1)=\gamma_{\mu\mathbf{c}0}+\gamma_{\mu\mathbf{c}1}\cos(Qn+\phi)\ . \tag{11}$$

For the normal phase we have simply $\alpha_{\mu1}=\gamma_{\mu\mathbf{c}1}=0$.

In terms of these matrix elements, the Schrödinger equation (5) can be expressed as

$$[E_\mu(\mathbf{k})-\alpha_\mu(n)-2\gamma_{\mu\mathbf{a}}\cos(\mathbf{k}\cdot\mathbf{a})-2\gamma_{\mu\mathbf{b}}\cos(\mathbf{k}\cdot\mathbf{b})]F_{\mu\mathbf{k}}(n)=e^{-i\mathbf{k}\cdot\mathbf{c}}\gamma_{\mu\mathbf{c}}(n,n-1)F_{\mu\mathbf{k}}(n-1)+e^{i\mathbf{k}\cdot\mathbf{c}}\gamma_{\mu\mathbf{c}}(n+1,n)F_{\mu\mathbf{k}}(n+1)\ . \tag{12}$$

For a pure one-dimensional system, we have $\gamma_{\mu\mathbf{a}}=0$ and $\gamma_{\mu\mathbf{b}}=0$. If the amplitude of the on site modulation $\alpha_{\mu1}$ is set equal to zero we will obtain the model used by Raising[6]

$$[E_\mu(\mathbf{k})-\alpha_{\mu0}]F_{\mu\mathbf{k}}(n)=e^{-i\mathbf{k}\cdot\mathbf{c}}\gamma_{\mu\mathbf{c}}(n,n-1)F_{\mu\mathbf{k}}(n-1)+e^{i\mathbf{k}\cdot\mathbf{c}}\gamma_{\mu\mathbf{c}}(n+1,n)F_{\mu\mathbf{k}}(n+1)\ . \tag{13}$$

If we further set $\gamma_{\mu\mathbf{c}1}=0$, Eq. (12) reduces to the Aubry model[8]

$$[E_\mu(\mathbf{k})-\alpha_{\mu0}-\alpha_{\mu1}\cos(Qn+\phi)]F_{\mu\mathbf{k}}(n)=e^{-i\mathbf{k}\cdot\mathbf{c}}\gamma_{\mu\mathbf{c}0}F_{\mu\mathbf{k}}(n-1)+e^{i\mathbf{k}\cdot\mathbf{c}}\gamma_{\mu\mathbf{c}0}F_{\mu\mathbf{k}}(n+1)\ . \tag{14}$$

However, we will show in the later sections that these one-dimensional models cannot explain satisfactorily the optical transmission experiment.

## III. THE ELECTRONIC STATES

The purpose of this paper is not to perform an energy band calculation, but to demonstrate the characteristic change of the transmission spectrum when $Rb_2ZnBr_4$ undergoes a normal-to-incommensurate structure phase transition. For this purpose, it is sufficient to consider for the normal phase a simple conduction band ($\mu=c$) with $\gamma_{c\mathbf{a}}=\gamma_{c\mathbf{b}}=\gamma_{c\mathbf{c}0}=-2$ and $\alpha_{c0}=60$, and a simple valence band ($\mu=v$) with $\gamma_{v\mathbf{a}}=\gamma_{v\mathbf{b}}=\gamma_{v\mathbf{c}0}=1$ and $\alpha_{v0}=0$. So the normal phase is described by a conduction band

$$E_c(\mathbf{k})=60-4\cos(\mathbf{k}\cdot\mathbf{a})-4\cos(\mathbf{k}\cdot\mathbf{b})-4\cos(\mathbf{k}\cdot\mathbf{c}) \tag{15}$$

and a valence band

$$E_v(\mathbf{k})=2\cos(\mathbf{k}\cdot\mathbf{a})+2\cos(\mathbf{k}\cdot\mathbf{b})+2\cos(\mathbf{k}\cdot\mathbf{c}) \tag{16}$$

with a band gap 42 at $\mathbf{k}=\mathbf{0}$. To derive the energy bands of the incommensurate phase which is specified by the modulations, Eqs. (10) and (11), we must first fix the values of $\alpha_{\mu1}$, $\gamma_{\mu\mathbf{c}1}$, $Q$, and $\phi$, and then solve the Schrödinger equation (12). Within the rational approximation $Q=2\pi(\nu/N)$, each of the conduction bands and the valence bands of the normal phase will split into $N$ subbands. For convenience we will use the reduced zone scheme and label the subbands by $(\mu,\eta)$, where $\mu=c$ or $v$, and $\eta=1,2,\ldots,N$. Consequently, the energy bands are represented by $E_{\mu\eta}(\mathbf{k})$ and the Bloch states given by Eq. (3) are expressed as $\Psi_{\mu\eta\mathbf{k}}(\mathbf{r})$ with the corresponding coefficients $F_{\mu\eta\mathbf{k}}(n)$.

Knowing the complete energy spectra we can calculate the dielectric function to study the optical absorption. We will show in the next section that the imaginary part of the dielectric function is proportional to the following quantity:

$$\Gamma(\omega)=\int d\mathbf{k}\sum_{\eta,\xi}\left|\sum_{n}F^{*}_{c\eta\mathbf{k}}(n)F_{v\xi\mathbf{k}}(n)\right|^{2}\times\delta(E_{c\eta}(\mathbf{k})-E_{v\xi}(\mathbf{k})-\hbar\omega)\ , \tag{17}$$

where the integration runs over the reduced Brillouin zone. In this section we will investigate the effect of band split on $\Gamma(\omega)$ when the normal-to-incommensurate phase transition occurs.

We will start with the normal phase. Because the energy bands given by Eqs. (15) and (16) have the simple symmetry relation $E_c(\mathbf{k})-30=-[2E_v(\mathbf{k})-30]$, $\Gamma(\omega)$ turns out to be symmetric with respect to $\hbar\omega=60$. In Fig. 1, $\Gamma(\omega)$ for the normal phase is plotted as curve $N$. Because of the symmetry, in Fig. 1, we only plot the left half of the $\Gamma(\omega)$ function.

For the incommensurate phase the shape of $\Gamma(\omega)$ varies with the modulation parameters $\alpha_{\mu 1}$, $\gamma_{\mu c1}$, $Q$, and $\phi$. We found that the numerical result is very insensitive to the value of $\phi$, and so we can use any arbitrary phase. Let us first choose the values of $\alpha_{\mu 1}$ and $\gamma_{\mu c1}$ such that the resultant band structure has the same normal phase symmetry $E_c(\mathbf{k})-30=-[2E_v(\mathbf{k})-30]$. Under this symmetry condition $\Gamma(\omega)$ is again symmetric with respect to $\hbar\omega=60$. The first case to be considered is the pure site-energy modulation with $\alpha_{c1}=-4$, $\alpha_{v1}=2$, $\gamma_{cc1}=\gamma_{vc1}=0$, and $Q=2\pi(0.292)\approx 2\pi(\frac{5}{17})$. With this set of parameters, Eq. (12) is solved numerically for the energy bands $E_{\mu\eta}(\mathbf{k})$ and the Bloch states $\Psi_{\mu\eta\mathbf{k}}(\mathbf{r})$. We order the subbands of the conduction band ($\mu=c$) as $E_{c\eta}(\mathbf{k})>E_{c\xi}(\mathbf{k})$ if $\eta>\xi$, and the subbands of the valence band ($\mu=v$) as $E_{v\eta}(\mathbf{k})>E_{v\xi}(\mathbf{k})$ if $\eta<\xi$. Because of the above-mentioned mirror-image-type symmetry, Eq. (17) reduces to

$$\Gamma(\omega)=\sum_{\eta}\Gamma_{\eta}(\omega)\ , \tag{18}$$

where

$$\Gamma_{\eta}(\omega)=\int d\mathbf{k}\left|\sum_{n}F^{*}_{c\eta\mathbf{k}}(n)F_{v\eta\mathbf{k}}(n)\right|^{2}\times\delta(E_{c\eta}(\mathbf{k})-E_{v\eta}(\mathbf{k})-\hbar\omega)\ . \tag{19}$$

Since the reciprocal lattice vector of the reduced zone along the $\mathbf{c}^*$ axis is only $\frac{1}{17}$ of its original value, each subband is very flat along the $\mathbf{c}^*$ axis and $E_{\mu\eta}(\mathbf{k})$ is characteristic of a two-dimensional tight-binding band. Consequently, all $\Gamma_{\eta}(\omega)$ have similar shape. As an example, $\Gamma_1(\omega)$ is plotted in Fig. 1 as curve $A1$. The lower edges of all the 17 $\Gamma_{\eta}(\omega)$ with $\eta=1,2,\ldots,17$ are marked by arrowheads. $\Gamma(\omega)$ is then the superposition of all these 17 $\Gamma_{\eta}(\omega)$, shown as curve $A$. If we improve the rational approximation to have $Q\approx 2\pi(\frac{17}{57})$, the computed $\Gamma(\omega)$ is given in Fig. 1 as curve $B$. Except for the slight roundup of the stepped structure as a result of the secondary band split, curves $B$ and $A$ have similar characteristic features. We would like to point out that the large shift of the lower edge of $\Gamma(\omega)$ due to the pure site-energy modulation has a strong effect on the threshold of optical absorption.

The second case to be considered under the symmetry condition $E_c(\mathbf{k})-30=-[2E_v(\mathbf{k})-30]$ is the pure hopping modulation with $\alpha_{c1}=\alpha_{v1}=0$, $\gamma_{cc1}=1$, and

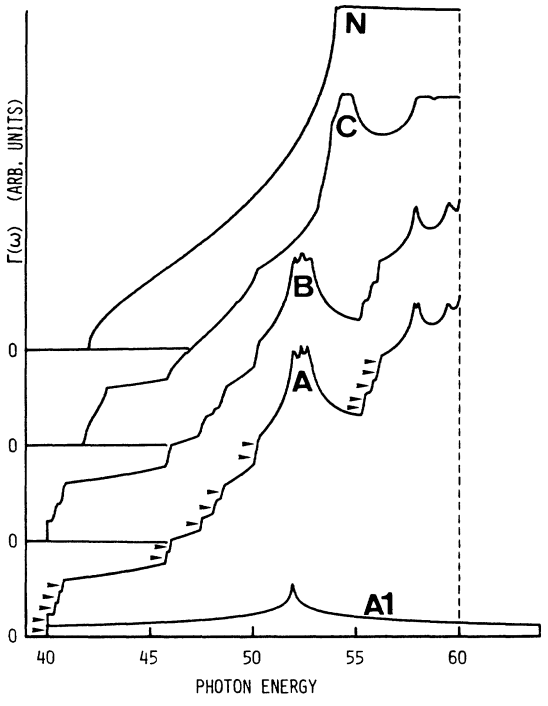


FIG. 1. The $\Gamma(\omega)$ function for the normal phase and the incommensurate phase with various types of modulations. The curves $N$, $C$, $B$, and $A$ are symmetric with respect to the photon energy equal to 60. The units of photon energy are determined by setting $\hbar\omega=42$ equal to the band gap. For $Rb_2ZnBr_4$, the band gap is 5 eV. The same energy units are used in all figures.

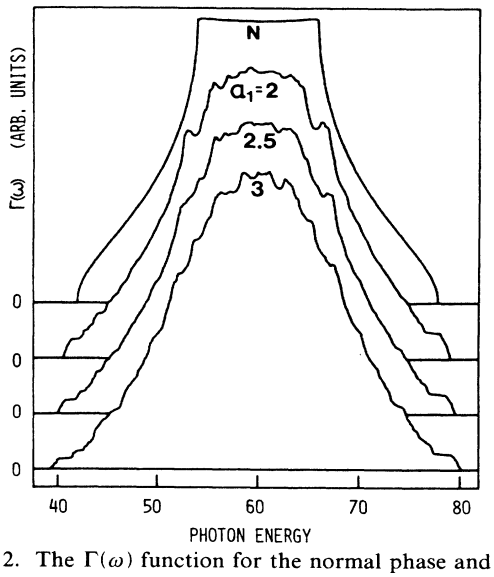


FIG. 2. The $\Gamma(\omega)$ function for the normal phase and the incommensurate phase with various types of modulations. Only the normal phase (curve $N$) is symmetric with respect to the photon energy equal to 60.

$\gamma_{vc1}=-0.5$. The signs of $\gamma_{cc1}$ and $\gamma_{vc1}$ are so chosen that the absolute value of each hopping matrix element decreases with increasing interatomic distance. We again solve Eq. (12) with $Q\approx 2\pi(\frac{5}{17})$ and compute $\Gamma(\omega)$ from Eq. (17). The so obtained $\Gamma(\omega)$ is shown in Fig. 1 as curve $C$. Although each of the conduction and the valence bands split also into 17 subbands, the shift of the lower edge of $\Gamma(\omega)$ due to the pure hopping modulation is negligibly small. Therefore, such modulation has only a rather weak effect on the threshold of optical absorption spectra.

Finally, we study the general case of having both the site-energy modulation $\alpha_{c1}=\alpha_{v1}=\alpha_1$ and the hopping modulation $\gamma_{cc1}=1$ and $\gamma_{vc1}=-0.5$. With the rational approximation $Q\approx 2\pi(\frac{5}{17})$, the calculated $\Gamma(\omega)$ is shown in Fig. 2 for $\alpha_1=2$, 2.5, and 3, together with the $\Gamma(\omega)$ of the normal phase. Because the mirror-image-type symmetry $E_c(\mathbf{k})-30=-[2E_v(\mathbf{k})-30]$ is now destroyed, Eq. (18) is no longer valid and there are many mixed-subband transitions ($\xi\neq\eta$) contributing to the $\Gamma(\omega)$ given by Eq. (17). Consequently, the shape of $\Gamma(\omega)$ in Fig. 2 is quite different from the shape of $\Gamma(\omega)$ in Fig. 1.

Although Figs. 1 and 2 are obtained with $\gamma_{ca}=\gamma_{cb}=\gamma_{cc0}=-2$, $\alpha_{c0}=60$, $\gamma_{va}=\gamma_{vb}=\gamma_{vc0}=1$, and $\alpha_{v0}=0$, we have repeated the calculations with other choices of parameter values. We found that as long as the absolute values of the six $\gamma$ parameters are of the same order of magnitude, there is no qualitative change of the calculated $\Gamma(\omega)$ shown in Fig. 2. In other words, the curves in Fig. 2 exhibit characteristic features of the three-dimensional model.

Before we close this section, we would like to comment on the even simpler case which assumes $Q\approx 2\pi(\frac{1}{3})$ and the mirror-image-type symmetry of the band structure. If we inspect curve $A$ in Fig. 1, we see that the 17 $\Gamma_\eta(\omega)$ separate themselves into three groups: $\eta=1$ to $\eta=5$ for the first group, $\eta=6$ to $\eta=12$ for the second group, and $\eta=13$ to $\eta=17$ for the third group. The corresponding 17 subbands also group themselves into three energy intervals separated by gaps of the size $\Delta E_g\approx 6$. If we use $Q\approx 2\pi(\frac{1}{3})$ instead of $Q\approx 2\pi(\frac{5}{17})$, then all the subbands in each energy interval collapse into one single subband. In this case, the fine stepped structure marked by arrowheads in Fig. 1 is washed out. Instead of 17 small steps, curve $A$ in Fig. 1 will only have three giant steps. We will return to this point later when we discuss the optical absorption spectra.

## IV. INTERBAND OPTICAL ABSORPTION

The theory of interband optical absorption is well established and can be found in many books. Here we will only outline the key points which are essential for our calculation.

In the presence of an electromagnetic field, the single-particle Hamiltonian Eq. (1) is modified as

$$H=(\tfrac{1}{2}m)[\mathbf{p}-(e/c)\mathbf{A}]^2+V(\mathbf{r}) , \tag{20}$$

where $\mathbf{A}$ is the vector potential. The probability of direct optical transitions from the $(v\xi)$ subband to the $(c\eta)$ subband has been derived with the time-dependent perturbation theory and is known as the golden rule:

$$W(\omega)=(\tfrac{1}{2}\pi^2\hbar)\int d\mathbf{k}\,|\langle\Psi_{c\eta\mathbf{k}}(\mathbf{r})|(e/mc)\mathbf{A}\cdot\mathbf{p}|\Psi_{v\xi\mathbf{k}}(\mathbf{r})\rangle|^2\delta(E_{c\eta}(\mathbf{k})-E_{v\xi}(\mathbf{k})-\hbar\omega) . \tag{21}$$

Since the electromagnetic field induces an ac current in the material, the absorbed photon energy per unit time $W(\omega)\hbar\omega$ is equal to the rate of energy loss $(\frac{1}{2})\sigma(\omega)E_0^2$ due to Joule heating, where $\sigma(\omega)$ is the ac conductivity and $E_0$ is the amplitude of the electric field. One can find in textbook the relation $\sigma(\omega)=(\omega/4\pi)\epsilon_2(\omega)$ between the ac conductivity and the imaginary part of the dielectric function $\epsilon_2(\omega)$. Therefore, if we solve Eq. (14) and then obtain the Bloch state from Eq. (3), $\epsilon_2(\omega)$ can be calculated from

$$\epsilon_2(\omega)=(1/\pi)(e/m\,\Omega\omega)^2\,|\langle\Phi_c(\mathbf{r})|\hat{\mathbf{e}}\cdot\mathbf{p}|\Phi_v(\mathbf{r})\rangle|^2\int d\mathbf{k}\sum_{n,\xi}\left|\sum_n F^*_{c\eta\mathbf{k}}(n)F_{v\xi\mathbf{k}}(n)\right|^2\delta(E_{c\eta}(\mathbf{k})-E_{v\xi}(\mathbf{k})-\hbar\omega) , \tag{22}$$

where $\Omega=\mathbf{a}\cdot(\mathbf{b}\times\mathbf{c})$ and $\hat{\mathbf{e}}$ is the photon polarization vector. Substituting Eq. (17) into Eq. (22), we have

$$\epsilon_2(\omega)=(1/\pi)(e/m\,\Omega\omega)^2\,|\langle\Phi_c(\mathbf{r})|\hat{\mathbf{e}}\cdot\mathbf{p}|\Phi_v(\mathbf{r})\rangle|^2\,\Gamma(\omega) . \tag{23}$$

We want to calculate the transmission coefficient $T(\omega)$ of a slab sample of thickness $d$, with a normal incident electromagnetic wave of frequency $\omega$. Let

$$N(\omega)=\nu(\omega)+i\kappa(\omega) \tag{24}$$

be the complex index of refraction of the slab sample. The fundamental theory of electromagnetic wave propagation gives the transmission coefficient as

$$T(\omega)=\frac{[1-R(\omega)]^2+4R(\omega)\sin^2(\theta)}{[1-R(\omega)S(d,\omega)]^2+4R(\omega)S(d,\omega)\sin^2(\theta+\beta)}S(d,\omega) , \tag{25}$$

where

$$R(\omega)=\frac{|\nu(\omega)-1+i\kappa(\omega)|^2}{|\nu(\omega)+1+i\kappa(\omega)|^2}\ , \tag{26}$$

$$S(d,\omega)=\exp[-2\omega\kappa(\omega)d/c]\ , \tag{27}$$

$$\tan(\theta)=\frac{2\kappa(\omega)}{\nu(\omega)^2+\kappa(\omega)^2-1}\ , \tag{28}$$

and

$$\beta=(1/c)\omega\nu(\omega)d\ . \tag{29}$$

For a real slab sample the two surfaces are not perfectly parallel to each other. Hence, the slight variation of the sample thickness should be averaged over.[16] If we redefine $d$ as the mean thickness of the sample, the average-corrected transmission coefficient is then simply

$$T(\omega)=\frac{[1-R(\omega)]^2\{1+[\kappa(\omega)/\nu(\omega)]^2\}}{1-R(\omega)^2S(d,\omega)^2}S(d,\omega)\ . \tag{30}$$

The refractive index $\nu(\omega)$ and the extinction coefficient $\kappa(\omega)$ are related to the real part $\epsilon_1(\omega)$ and the imaginary part $\epsilon_2(\omega)$ of the dielectric function as

$$\epsilon_1(\omega)=\nu(\omega)^2-\kappa(\omega)^2\ , \tag{31}$$

$$\epsilon_2(\omega)=2\nu(\omega)\kappa(\omega)\ . \tag{32}$$

Since $\Gamma(\omega)$ was already computed in the previous section, $\epsilon_2(\omega)$ can be calculated from Eq. (23) with the constant matrix element $\langle\Phi_c(\mathbf{r})|\hat{\mathbf{e}}\cdot\mathbf{p}|\Phi_v(\mathbf{r})\rangle$ determined by fitting the peak value of the calculated $\epsilon_2(\omega)$ to the peak value of the measured $\epsilon_2(\omega)$ in the normal phase. Knowing the imaginary part $\epsilon_2(\omega)$, the real part $\epsilon_1(\omega)$ is then derived from using the Kramers-Kronig relations. Finally, the transmission coefficient $T(\omega)$ is obtained from Eq. (30) with the help of Eqs. (31) and (32).

Figure 3 shows the calculated transmission spectra for the normal phase (curve $N$), the incommensurate phase with pure site-energy modulation (curve $A$), and the incommensurate phase with pure hopping modulation (curve $C$). These curves are derived with the same values of parameters as those used in calculating the corresponding curves in Fig. 1. The stepped structure of the transmission spectra of the incommensurate phases is caused by the similar stepped structure of the $\Gamma(\omega)$ curves in Fig. 1. As an explicit example, the corresponding steps of the $T(\omega)$ spectrum in Fig. 3 (curve $A$) and of the $\Gamma(\omega)$ spectrum in Fig. 1 (curve $A$) are marked by arrowheads.

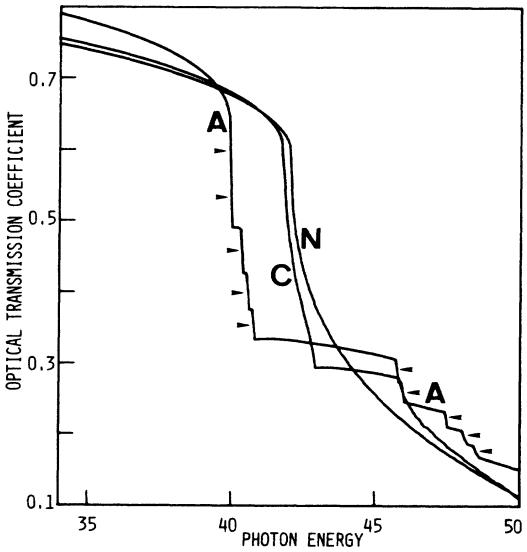


FIG. 3. Optical transmission spectra for the phase of Fig. 1.

When we include both the site-energy modulation and the hopping modulation in the incommensurate phase, the calculated transmission spectra are given in Fig. 4 (curves $\alpha_1=3$, 2.5, and 2) together with the transmission spectrum of the normal phase (curve $N$). These four curves and the four corresponding $\Gamma(\omega)$ spectra in Fig. 2 are calculated with the same values of parameters. The inset in Fig. 4 is the measured transmission spectra[6] for the normal phase (3 K above the transition temperature $T_I\approx355$ K), and for the incommensurate phase at three different temperatures $T=T_I-3$, $T_I-33$, and $T_I-56$. In our calculation the band gap of the normal phase is at $\hbar\omega=42$, corresponding to the measured gap 5 eV. Since the modulation strength gets stronger with increasing $T_I-T$ (for the experiment) and with increasing values of $\alpha_1$ (for the theory), the calculated $T(\omega)$ in Fig. 4 reproduces the main features of the experimental observation.

However, in Fig. 4 the experimental results are far smoother than the theoretical ones. There are several reasons for this discrepancy. We have used the rational approximation $Q\approx2\pi(\frac{5}{17})$. As we mentioned in Sec. III in connection to the stepped structure of $\Gamma(\omega)$ in Fig. 1, the sharpness of these steps, the number of these steps, and the size of these steps depend on the denominator of the rational approximation. If we use the sequence of rational approximation $Q\approx2\pi(\frac{1}{3})$, $Q\approx2\pi(\frac{5}{17})$, and $Q\approx2\pi(\frac{17}{57})$, then the calculated transmission spectra become smoother. Nevertheless, such improvement is not significant. As long as we use the simple model of tight-binding band, most likely, the appearance of the stepped structure in $T(\omega)$ cannot be avoided. On the

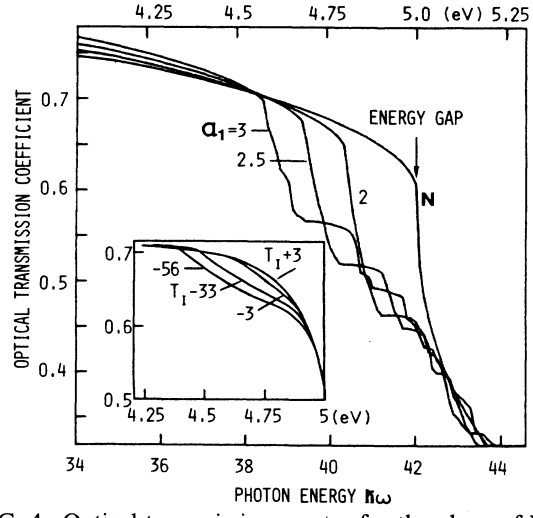


FIG. 4. Optical transmission spectra for the phase of Fig. 2. Inset is the experimental curves for various temperatures.

other hand, in the paper which reported the experimental results,[6] one also finds the raw data of the temperature dependence of absorption increase $\Delta\alpha$ in the incommensurate phase (Fig. 2 of Ref. 6). The raw data do not follow a smooth curve. Without further experimental information, we should not claim better agreement between the theory and the experiment than what is shown in Fig. 4.

By comparing the transmission spectra in Fig. 3 with experimental results in Fig. 4, it is clear that a simpler incommensurate model including either pure site-energy modulation or pure hopping modulation cannot be realistic. In the following we will demonstrate that a quasi-one-dimensional model yields even worse result.

## V. REMARKS

Rasing[6] has studied the optical absorption of $Rb_2ZnBr_4$ with a one-dimensional incommensurate model Hamiltonian. Here we will investigate a more realistic case: A crystal with strong uniaxial anisotropy along the direction of incommensurate modulation. Such a system can be reached by reducing the transverse hopping matrix elements $\gamma_{\mu a}$ and $\gamma_{\mu b}$ defined by Eqs. (8) and (9). Therefore, we specify the quasi-one-dimensional normal phase by the parameters $\gamma_{ca}=\gamma_{cb}=(\frac{1}{10})\gamma_{cc0}=-0.2$, $\gamma_{va}=\gamma_{vb}=(\frac{1}{10})\gamma_{vc0}=0.1$, $\alpha_{c0}=60$, and $\alpha_{v0}=0$. With the rational approximation $Q\approx 2\pi(\frac{5}{17})$, the calculated $\Gamma(\omega)$ function and the transmission spectrum $T(\omega)$ of the normal phase are shown as curve $N$ in Figs. 5 and 6, respectively.

Next, we consider the incommensurate phase with pure hopping modulation $\alpha_{c1}=\alpha_{v1}=0$, $\gamma_{cc1}=1$, and $\gamma_{vc1}=-0.5$. The $\Gamma(\omega)$ function of this incommensurate phase is given in Fig. 5 as curve $C$. The calculated transmission spectrum, shown as curve $C$ in Fig. 6, is slightly shifted from the normal phase spectrum.

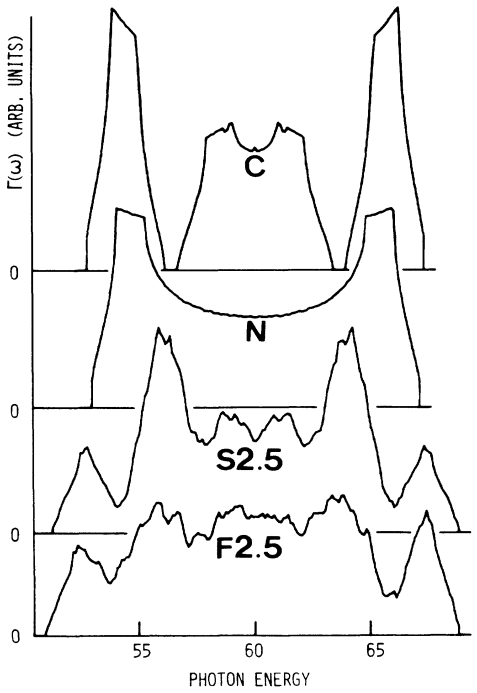


FIG. 5. $\Gamma(\omega)$ function for the normal phase and the incommensurate phase with various types of modulations in a quasi-one-dimensional system.

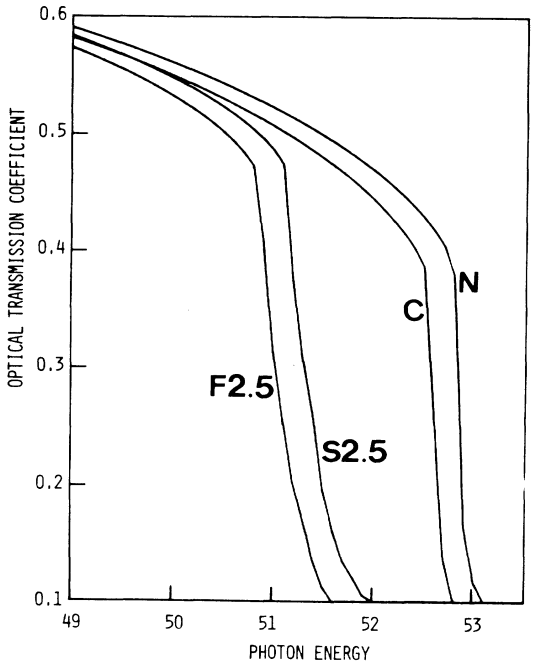


FIG. 6. Optical transmission spectra for the phases in Fig. 5. The system is quasi-one-dimensional.

For the incommensurate phase with pure site-energy modulation, we set $\gamma_{cc1}=\gamma_{vc1}=0$ and $\alpha_{c1}=\alpha_{v1}=2.5$. The curves marked as $S$ 2.5 in Figs. 5 and 6 are the calculated $\Gamma(\omega)$ function and the transmission spectrum $T(\omega)$. Finally, we study the general case of full modulation with $\gamma_{cc1}=1$, $\gamma_{vc1}=-0.5$, and $\alpha_{c1}=\alpha_{v1}=2.5$. Then we obtain the $\Gamma(\omega)$ function shown in Fig. 5 as curve $F2.5$, and the transmission spectrum $T(\omega)$ shown in Fig. 6 also as curve $F2.5$.

Obviously, Fig. 6 for the quasi-one-dimensional system is entirely different from the observed behavior of $T(\omega)$ when the system undergoes the normal-to-incommensurate structure phase transition.

To close this paper, we would like to emphasize that although the explicit numerical results shown here are derived with specific values of the parameters, we have calculated the transmission spectra with many other parameter values. The characteristic features of the observed spectra can be reproduced only if we use a three-dimensional system with a uniaxial incommensurate modulation in both site-energy and hopping matrix elements. As long as this requirement is fulfilled, the qualitative features of the calculated transmission spectra are not sensitive to the choice of parameter values.

## ACKNOWLEDGMENT

This work was financially supported by the Swedish Natural Science Research Council under Grant No. NFR-FFU-3996-141.

[1]R. Blinc, Phys. Rep. **79**, 331 (1981).
[2]C. J. de Pater and C. van Dijk, Phys. Rev. B **18**, 1281 (1978).
[3]Th. Rasing, J. H. M. Stoelinga, and P. Wyder, Solid State Commun. **35**, 229 (1980).
[4]M. Iizumi and K. Gesi, J. Phys. Soc. Jpn. **52**, 2526 (1983).
[5]Th. Rasing, Ph.D. thesis, University of Nijmegen, 1982 (unpublished).
[6]Th. Rasing, Phys. Rev. Lett. **53**, 388 (1984).
[7]For a review, see J. B. Sokoloff, Phys. Rep. **126**, 189 (1985).
[8]S. Aubry and C. André, Ann. Isr. Phys. Soc. **3**, 133 (1980).
[9]C. M. Soukoulis and E. N. Economou, Phys. Rev. Lett. **48**, 1043 (1982).
[10]D. R. Grempel, S. Fishman, and R. E. Prange, Phys. Rev. Lett. **49**, 833 (1982).
[11]D. R. Hofstadter, Phys. Rev. B **14**, 2239 (1976).
[12]S. Ostlund and R. Pandit, Phys. Rev. B **29**, 1394 (1984).
[13]I. M. Suslov, Zh. Eksp. Teor. Fiz. **83**, 1079 (1982) [Sov. Phys.—JETP **56**, 612 (1982)].
[14]K. A. Chao, R. Riklund and G. Wahlström, J. Phys. Lett. **18A**, 403 (1985).
[15]A. C. R. Hogervorst and P. M. de Wolff, Solid State Commun. **43**, 179 (1982).
[16]G. Harbeke, in *Optical Properties of Solids,* edited by F. Abeles (North-Holland, Amsterdam, 1972), p. 22.